PLOS ONE

RESEARCH ARTICLE

Darcy-Forchheimer flow with Cattaneo-Christov heat flux and homogeneous-heterogeneous reactions

Tasawar Hayat[1,2], Farwa Haider[1], Taseer Muhammad[1]*, Ahmed Alsaedi[2]

1 Department of Mathematics, Quaid-I-Azam University, Islamabad, Pakistan, **2** Nonlinear Analysis and Applied Mathematics (NAAM) Research Group, Department of Mathematics, Faculty of Science, King Abdulaziz University, Jeddah, Saudi Arabia

* taseer@math.qau.edu.pk

Citation: Hayat T, Haider F, Muhammad T, Alsaedi A (2017) Darcy-Forchheimer flow with Cattaneo-Christov heat flux and homogeneous-heterogeneous reactions. PLoS ONE 12(4): e0174938. https://doi.org/10.1371/journal.pone.0174938

Editor: Esmaiel Jabbari, University of South Carolina, UNITED STATES

Received: January 1, 2017

Accepted: March 17, 2017

Published: April 5, 2017

Data Availability Statement: All relevant data are within the paper.

Funding: The authors received no specific funding for this work.

Competing interests: The authors have declared that no competing interests exist.

Abstract

Here Darcy-Forchheimer flow of viscoelastic fluids has been analyzed in the presence of Cattaneo-Christov heat flux and homogeneous-heterogeneous reactions. Results for two viscoelastic fluids are obtained and compared. A linear stretching surface has been used to generate the flow. Flow in porous media is characterized by considering the Darcy-Forchheimer model. Modified version of Fourier's law through Cattaneo-Christov heat flux is employed. Equal diffusion coefficients are employed for both reactants and auto catalyst. Optimal homotopy scheme is employed for solutions development of nonlinear problems. Solutions expressions of velocity, temperature and concentration fields are provided. Skin friction coefficient and heat transfer rate are computed and analyzed. Here the temperature and thermal boundary layer thickness are lower for Cattaneo-Christov heat flux model in comparison to classical Fourier's law of heat conduction. Moreover, the homogeneous and heterogeneous reactions parameters have opposite behaviors for concentration field.

1. Introduction

Several industrial and environmental systems like geothermal energy systems, heat exchanger design, geophysics and catalytic reactors involve the convection flow subject to porous medium. The non-Darcian porous medium is the modified form of classical Darcian model which includes the inertia and boundary features. Flow subject to porous media is quite useful in building thermal insulation materials, beds of fossil fuels, energy storage units, nuclear waste disposal, solar receivers, heat exchanger, petroleum resources and numerous others [1–3]. The available literature witnesses that considerable attention has been given to modeling and analysis for flow subject to Darcy expression. The classical Darcy's law is valid under limited range of low velocity and smaller porosity. The Darcy's law is inadequate when inertial and boundary effects are accounted at higher flow rate. Due to such conditions it is impossible to ignore the effects of inertia and boundary. Forchheimer [4] included a square velocity term in the expression of Darcian velocity to predict the inertia and boundary features. Muskat [5] named this term as "Forchheimer term" which is always valid for high Reynolds number.

Seddeek [6] examined the impacts of thermophoresis and viscous dissipation in Darcy-Forchheimer mixed convective flow saturating non-Darcy porous medium. Pal and Mondal [7] employed the Darcy-Forchheimer theory to examine the hydromagnetic flow of variable viscosity liquid in a porous medium. Sadiq and Hayat [8] analyzed the Darcy-Forchheimer flow of Maxwell liquid bounded by a convectively heated surface. Shehzad et al. [9] employed the Darcy-Forchheimer flow of variable thermal conductivity Oldroyd-B liquid past a vertical sheet with nonlinear convection and heat flux through Cattaneo-Christov theory. Recently Hayat et al. [10] studied the Darcy-Forchheimer flow of Maxwell fluid subject to variable thermal conductivity and heat flux through Cattaneo-Christov theory.

At present the researchers are engaged in analyzing the mechanism of heat transfer as a wave rather than diffusion due to its enormous applications in nanofluid mechanics and skin burns [11–18]. Heat transfer is a natural process which occurs due to difference of temperature between the system or different components of same system. The fundamental law of heat conduction suggested by Fourier [19] is frequently employed for heat transfer characteristics from the time it showed up in literature. But one of the major limitations of this model is that it leads to a parabolic energy equation which means that an initial disturbance would instantly experience by the system under consideration. This fact is referred in literature as "paradox of heat conduction". To overcome this limitation, Cattaneo [20] modified this law by including relaxation time term. This term overcomes the paradox of heat conduction. Christov [21] further modified the Cattaneo theory [20] by changing the time derivative with Oldroyd upper-convected derivative. This theory is termed as Cattaneo-Christov heat flux theory. Straughan [22] used heat flux expression by Cattaneo-Christov theory to analyze the thermal convection in horizontal layer of viscous liquid. Ciarletta and Straughan [23] showed the structural stability and uniqueness of solutions for temperature equation by employing heat flux through Cattaneo-Christov theory. Haddad [24] studied thermal instability in Brinkman porous media by employing heat flux through Cattaneo-Christov expression. Mustafa [25] utilized the Cattaneo-Christov heat flux expression for rotating flow and heat transfer of Maxwell fluid. Hayat et al. [26] studied impact of Cattaneo-Christov heat flux in flow past a stretchable surface with variable thickness. Hayat et al. [27] also performed a comparative study for flows of viscoelastic materials by considering heat flux through Cattaneo-Christov expression. Waqas et al. [28] employed the heat flux by Cattaneo-Christov theory to examine the flow of variable thermal conductivity generalized Burgers fluid. Li et al. [29] studied the MHD viscoelastic flow and heat transfer past a vertical stretchable surface with Cattaneo-Christov heat flux. Recently Hayat et al. [30] analyzed three-dimensional flow of nanofluid subject to Cattaneo-Christov double diffusion.

Numerous chemically reacting structures involve the homogeneous and heterogenous reactions for example in catalysis, combustion and biochemical processes. Relation between the homogeneous and heterogeneous reactions is very complicated. There are various reactions which have the ability to progress slowly or not at all except in presence of a catalyst. Chemical reactions are employed in applications like fog formation and dispersion, food processing, ceramics and polymer production, hydrometallurgical industry and several others. Merkin [31] examined the homogeneous and heterogeneous reactions in flow of viscous liquid. He studied the homogeneous reaction for cubic autocatalysis and heterogeneous reaction on the catalyst surface. Homogenous and heterogeneous reactions with equal diffusivities are discussed by Chaudhary and Merkin [32]. Homogeneous-heterogeneous reactions in the stagnation-point flow towards a stretchable sheet are reported by Bachok et al. [33]. Homogeneous-heterogeneous reactions in flow of nanoliquid bounded by a porous stretchable surface is discussed by Kameswaran et al. [34]. Hayat et al. [35] studied melting heat in stretched flow of carbon nanotubes with homogeneous-heterogeneous reactions. Imtiaz et al. [36] explored

unsteady magnetohydrodynamic flow due to a curved stretchable surface with homogeneous and heterogeneous reactions. Hayat et al. [37] reported Cattaneo-Christov heat flux effect in Jeffrey fluid flow subject to homogeneous-heterogeneous reactions. Hayat et al. [38] also examined the effects of homogeneous-heterogeneous reactions in flow of nanofluids over a nonlinear stretchable sheet having variable thickness. Sajid et al. [39] explored the homogeneous-heterogeneous reactions in magnetohydrodynamic nanofluid flow by a curved surface. Tanveer et al. [40] analyzed the homogeneous-heterogeneous reactions in mixed convective peristaltic flow of Sisko fluid. Recently Hayat et al. [41] studied the homogeneous-heterogeneous reactions and convective conditions in boundary layer flow of nanofluid by a stretching cylinder embedded in a porous medium.

Main objective of this investigation is to construct a mathematical model for Darcy-Forchheimer boundary layer flow of viscoelastic fluids past a linear stretching surface. Flow models for elastico-viscous and second grade fluids [42–48] are taken into account. Impacts of Cattaneo-Christov heat flux and homogeneous-heterogeneous reactions are also studied. Boundary layer approach is used in the mathematical development. Appropriate variables lead to strong nonlinear ordinary differential system. Convergent series solutions for velocity, temperature and concentration fields are developed by using optimal homotopy analysis method (OHAM) [49–58]. The contributions of various pertinent parameters are studied and discussed. Further the skin friction coefficient and local Nusselt number have been computed and analyzed through numerical data.

2. Modeling

Let us consider two-dimensional (2D) flow of viscoelastic fluids bounded by a linear stretching surface with constant surface temperature. Incompressible viscoelastic fluids saturate the porous space characterizing Darcy-Forchheimer model. Here x – axis is parallel to stretchable surface while y – axis normal to x – axis. Let $u_w(x) = cx$ describes the stretching velocity along the x – direction. Homogeneous and heterogeneous reactions of two chemical species A and B are accounted. Heat transfer mechanism is employed through Cattaneo-Christov heat flux theory. Homogeneous reaction for cubic autocatalysis is [36, 38]:

$$A + 2B \rightarrow 3B, \;\; rate = k_c ab^2, \tag{1}$$

while the heterogeneous reaction on the catalyst surface has been expressed by

$$A \rightarrow B, \;\; rate = k_s a, \tag{2}$$

where rate constants are denoted by k_c and k_s and the chemical species A and B have concentrations a and b respectively. The boundary layer equations governing the flow of viscoelastic fluids in the absence of viscous dissipation and thermal radiation can be written as follows [27, 38]:

$$\frac{\partial u}{\partial x} + \frac{\partial v}{\partial y} = 0, \tag{3}$$

$$u\frac{\partial u}{\partial x} + v\frac{\partial u}{\partial y} = \nu\frac{\partial^2 u}{\partial y^2} - k_0\left(u\frac{\partial^3 u}{\partial x \partial y^2} + v\frac{\partial^3 u}{\partial y^3} - \frac{\partial u}{\partial y}\frac{\partial^2 u}{\partial x \partial y} + \frac{\partial u}{\partial x}\frac{\partial^2 u}{\partial y^2}\right) - \frac{\nu}{K^*}u - Fu^2, \tag{4}$$

$$\rho c_p\left(u\frac{\partial T}{\partial x} + v\frac{\partial T}{\partial y}\right) = -\nabla.\mathbf{q}, \tag{5}$$

$$u\frac{\partial a}{\partial x}+v\frac{\partial a}{\partial y}=D_A\frac{\partial^2 a}{\partial y^2}-k_c ab^2, \tag{6}$$

$$u\frac{\partial b}{\partial x}+v\frac{\partial b}{\partial y}=D_B\frac{\partial^2 b}{\partial y^2}+k_c ab^2. \tag{7}$$

Note that u and v denote the fluid velocities in $x-$ and $y-$directions respectively while $\nu\,(=\mu/\rho)$, μ and ρ stand for kinematic viscosity, dynamic viscosity and density of base liquid respectively, $k_0=-\alpha_1/\rho$ for elastic parameter, T for temperature, K^* for permeability of porous media, $F=C_b/xK^{*1/2}$ for non-uniform inertia coefficient of porous medium, C_b for drag coefficient and $\mathbf{q}$ for heat flux. Here $k_0>0$ represents elastico-viscous fluid, $k_0<0$ is for second grade fluid and $k_0=0$ for Newtonian fluid. According to Cattaneo-Christov heat flux theory, we have [21, 27]:

$$\mathbf{q}+\lambda\left(\frac{\partial\mathbf{q}}{\partial t}+\mathbf{V}.\nabla\mathbf{q}-\mathbf{q}.\nabla\mathbf{V}+(\nabla.\mathbf{V})\,\mathbf{q}\right)=-k\nabla T, \tag{8}$$

where k stands for thermal conductivity and λ for relaxation time of heat flux. Classical Fourier's law is deduced by putting $\lambda=0$ in Eq (8). By considering the incompressibility condition ($\nabla.\mathbf{V}=0$) and steady flow with $(\frac{\partial q}{\partial t}=0)$, Eq (8) becomes [21, 27]:

$$\mathbf{q}+\lambda(\mathbf{V}.\nabla\mathbf{q}-\mathbf{q}.\nabla\mathbf{V})=-k\nabla T. \tag{9}$$

Then the energy equation takes the following form [21, 27]:

$$u\frac{\partial T}{\partial x}+v\frac{\partial T}{\partial y}+\lambda\Phi_E=\alpha\left(\frac{\partial^2 T}{\partial y^2}\right), \tag{10}$$

$$\Phi_E=u\frac{\partial u}{\partial x}\frac{\partial T}{\partial x}+v\frac{\partial v}{\partial y}\frac{\partial T}{\partial y}+u\frac{\partial v}{\partial x}\frac{\partial T}{\partial y}+v\frac{\partial u}{\partial y}\frac{\partial T}{\partial x}+2uv\frac{\partial^2 T}{\partial x\partial y}+u^2\frac{\partial^2 T}{\partial x^2}+v^2\frac{\partial^2 T}{\partial y^2}. \tag{11}$$

The associated boundary conditions are [27, 38]:

$$u=u_w(x)=cx,\quad v=0,\quad T=T_w,\quad D_A\frac{\partial a}{\partial y}=k_s a,\quad D_B\frac{\partial b}{\partial y}=-k_s a\ \text{ at }\ y=0, \tag{12}$$

$$u\to 0,\quad T\to T_\infty,\quad a\to a_0,\quad b\to 0\ \text{ as }\ y\to\infty, \tag{13}$$

in which $\alpha=k/(\rho c_p)$ stands for thermal diffusivity, D_A and D_B for diffusion coefficients, T_w for constant surface temperature, T_∞ for ambient fluid temperature and c for positive stretching rate constant with T^{-1} as the dimension. Selecting

$$\begin{aligned} &u=cxf'(\zeta),\ \ v=-(c\nu)^{1/2}f(\zeta),\ \ \zeta=\left(\frac{c}{\nu}\right)^{1/2}y,\\ &\theta(\zeta)=\frac{T-T_\infty}{T_w-T_\infty},\ \ a=a_0\phi(\zeta),\ \ b=a_0h(\zeta). \end{aligned} \tag{14}$$

Continuity equation is trivially satisfied and Eqs (4)–(13) become

$$f''' + ff'' - k_1^*(2f'f''' - f''^2 - ff^{iv}) - \lambda f' - (1 + F_r)f'^2 = 0, \tag{15}$$

$$\frac{1}{\Pr}\theta'' + f\theta' - \gamma(ff'\theta' + f^2\theta'') = 0, \tag{16}$$

$$\frac{1}{Sc}\phi'' + f\phi' - K\phi h^2 = 0, \tag{17}$$

$$\frac{\delta}{Sc}h'' + fh' + K\phi h^2 = 0, \tag{18}$$

$$f = 0,\ f' = 1,\ \theta = 1,\ \phi\prime = K_s\phi,\ \delta h' = -K_s\phi \text{ at } \zeta = 0, \tag{19}$$

$$f' \to 0,\ \theta \to 0,\ \phi \to 1,\ h \to 0 \text{ as } \zeta \to \infty, \tag{20}$$

where k_1^* stands for viscoelastic parameter, λ for porosity parameter, F_r for inertia coefficient, Pr for Prandtl number, γ for thermal relaxation parameter, Sc for Schmidt number, K for strength of homogeneous reaction, δ for ratio of diffusion coefficients and K_s for strength of heterogeneous reaction. These parameters can be specified by using the definitions given below:

$$\left.\begin{aligned} k_1^* = -\frac{k_0 c}{\nu},\ \Pr = \frac{\nu}{\alpha},\ \gamma = c\lambda, \\ F_r = \frac{C_b}{K^{*1/2}},\ Sc = \frac{\nu}{D_A},\ K = \frac{k_c a_0^2}{u_w},\ K_s = \frac{k_s}{D_A a_0}\sqrt{\frac{\zeta}{\nu}},\ \delta = \frac{D_B}{D_A}. \end{aligned}\right\} \tag{21}$$

When $D_A = D_B$ then $\delta = 1$ and thus

$$\phi(\zeta) + h(\zeta) = 1. \tag{22}$$

Now Eqs (17) and (18) yield

$$\frac{1}{Sc}\phi'' + f\phi' - K\phi(1 - \phi)^2 = 0. \tag{23}$$

The subjected boundary conditions are

$$\phi'(0) = K_s\phi(0),\ \phi(\infty) \to 1. \tag{24}$$

Skin friction coefficient is defined as follows [27]:

$$C_f = \frac{\tau_w|_{y=0}}{\rho u_w^2} = \frac{\left(\nu\frac{\partial u}{\partial y} - k_0\left(u\frac{\partial^2 u}{\partial x \partial y} - 2\frac{\partial u}{\partial y}\frac{\partial v}{\partial y} + \nu\frac{\partial^2 u}{\partial y^2}\right)\right)_{y=0}}{u_w^2}. \tag{25}$$

Skin friction coefficient through dimensionless scale is

$$Re_x^{1/2} C_f = (1 - 3k_1^*)f''(0). \tag{26}$$

Local Nusselt number is given by

$$Re_x^{-1/2} Nu_x = -\theta'(0), \tag{27}$$

in which $\mathrm{Re}_x = u_w x/\nu$ depicts the local Reynolds number.

3. Solutions by OHAM

The series solutions of Eqs (15), (16) and (23) through the boundary conditions (19), (20) and (24) have been developed by employing optimal homotopy analysis technique (OHAM). Initial approximations and linear operators are

$$f_0(\zeta) = 1 - e^{-\zeta},\ \theta_0(\zeta) = e^{-\zeta},\ \phi_0(\eta) = 1 - \frac{1}{2}e^{-K_s\zeta}, \tag{28}$$

$$\mathbf{L}_f = \frac{d^3f}{d\zeta^3} - \frac{df}{d\zeta},\ \mathbf{L}_\theta = \frac{d^2\theta}{d\zeta^2} - \theta,\ \mathbf{L}_\phi = \frac{d^2\phi}{d\zeta^2} - \phi. \tag{29}$$

The above linear operators have the characteristics given as under

$$\mathbf{L}_f[C_1^{**} + C_2^{**}e^{\zeta} + C_3^{**}e^{-\zeta}] = 0,\ \mathbf{L}_\theta[C_4^{**}e^{\zeta} + C_5^{**}e^{-\zeta}] = 0,\ \mathbf{L}_\phi[C_6^{**}e^{\zeta} + C_7^{**}e^{-\zeta}] = 0, \tag{30}$$

in which C_j^{**} $(j = 1 - 7)$ stands for arbitrary constants.

4. Optimal convergence control parameters

Here the nonzero auxiliary parameters $\hbar_f$, $\hbar_\theta$ and $\hbar_\phi$ in homotopic solutions regulate the convergence region and also rate of homotopy solutions. To obtain the optimal values of $\hbar_f$, $\hbar_\theta$ and $\hbar_\phi$, we have employed the idea of minimization by defining the average squared residual errors as proposed by Liao [49].

$$\boldsymbol{\varepsilon}_m^f = \frac{1}{k+1}\sum_{j=0}^{k}\left[\mathbf{N}_f\left(\sum_{i=0}^{m}\hat{f}(\zeta)\right)_{\zeta=j\delta\zeta}\right]^2, \tag{31}$$

$$\boldsymbol{\varepsilon}_m^\theta = \frac{1}{k+1}\sum_{j=0}^{k}\left[\mathbf{N}_\theta\left(\sum_{i=0}^{m}\hat{f}(\zeta),\ \sum_{i=0}^{m}\hat{\theta}(\zeta)\right)_{\zeta=j\delta\zeta}\right]^2, \tag{32}$$

$$\boldsymbol{\varepsilon}_m^\phi = \frac{1}{k+1}\sum_{j=0}^{k}\left[\mathbf{N}_\phi\left(\sum_{i=0}^{m}\hat{f}(\zeta),\ \sum_{i=0}^{m}\hat{\phi}(\zeta)\right)_{\zeta=j\delta\zeta}\right]^2. \tag{33}$$

Following Liao [49]:

$$\boldsymbol{\varepsilon}_m^t = \boldsymbol{\varepsilon}_m^f + \boldsymbol{\varepsilon}_m^\theta + \boldsymbol{\varepsilon}_m^\phi, \tag{34}$$

where $\boldsymbol{\varepsilon}_m^t$ stands for total squared residual error, $\delta\zeta = 0.5$ and $k = 20$. The optimal values of convergence control parameters at 2nd order of approximations for elastico-viscous fluid case are $h_f = -1.53374$, $h_\theta = -1.30423$ and $h_\phi = -1.7072$ and total averaged squared residual error is $\boldsymbol{\varepsilon}_m^t = 7.6 \times 10^{-4}$ while the optimal values of convergence control parameters at 2nd order of approximations for second grade fluid case are $h_f = -1.04537$, $h_\theta = -1.29762$ and $h_\phi = -1.75305$ and total averaged squared residual error is $\boldsymbol{\varepsilon}_m^t = 6.6 \times 10^{-4}$. Figs 1 and 2 show the corresponding total residual error graphs. Tables 1 and 2 present the individual average squared residual errors using optimal values of convergence control parameters at $m = 2$. It is clearly observed that the averaged squared residual errors reduce with higher order approximations.

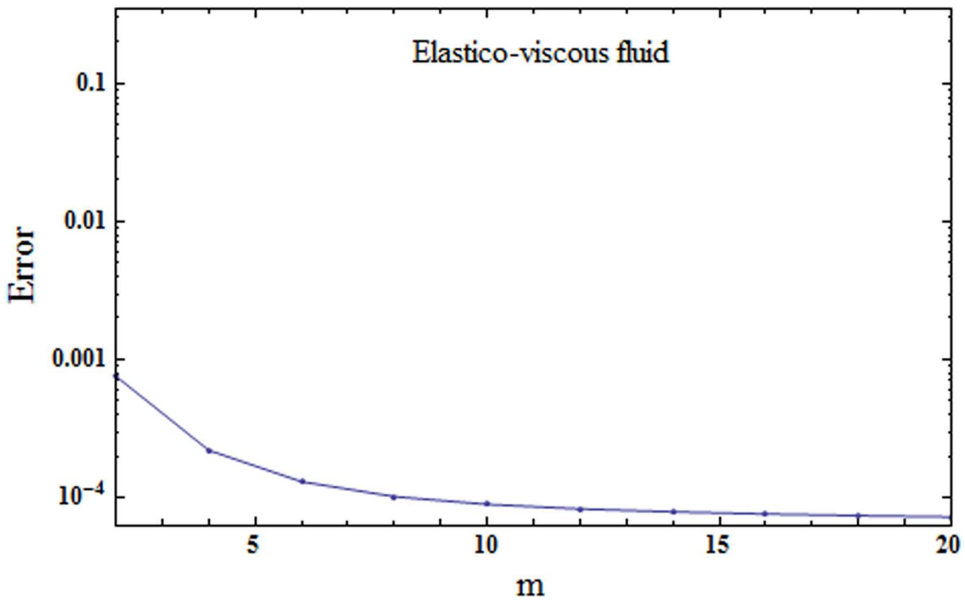

Fig 1. Total residual error for elastico-viscous fluid.

https://doi.org/10.1371/journal.pone.0174938.g001

5. Discussion

This section has been arranged to explore the effects of various influential parameters on the velocity $f'(\zeta)$, temperature $\theta(\zeta)$ and concentration $\phi(\zeta)$ distributions. Here the elastico-viscous $\left(k_1^* > 0\right)$ and second grade $\left(k_1^* < 0\right)$ fluids are considered. The computations have been carried out for various values of $k_1^*\left(-0.2 \leq k_1^* \leq 0.3\right)$, $\lambda(0.0 \leq \lambda \leq 0.7)$, F_r $(0.0 \leq F_r \leq 0.9)$, γ $(0.0 \leq \gamma \leq 0.5)$, $\mathrm{Pr}(0.7 \leq \mathrm{Pr} \leq 1.3)$, $Sc(0.5 \leq Sc \leq 1.5)$, $K(0.5 \leq K \leq 1.3)$ and $K_s(0.13 \leq K_s \leq 0.5)$ [59].

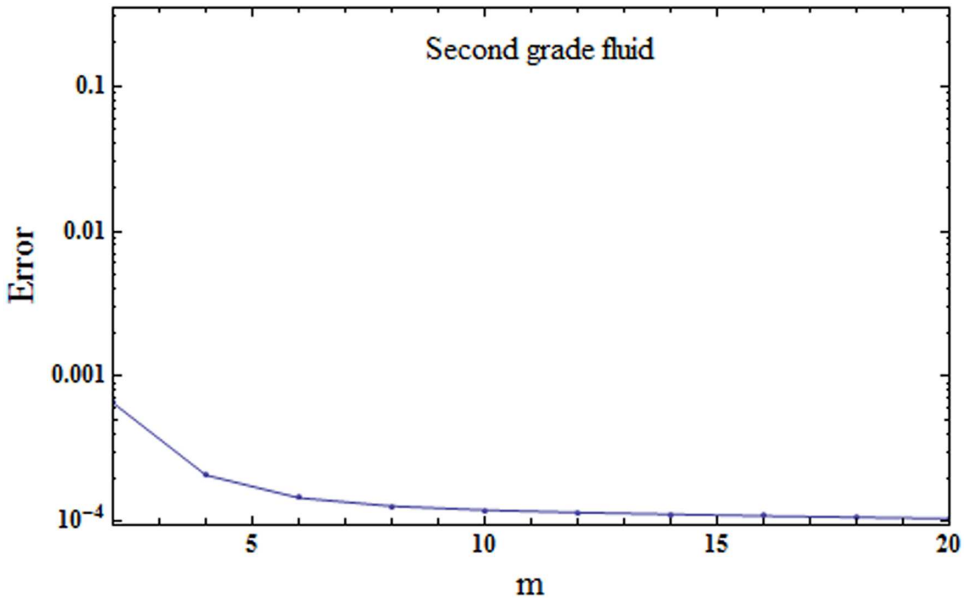

Fig 2. Total residual error for second grade fluid.

https://doi.org/10.1371/journal.pone.0174938.g002

Table 1. Individual averaged squared residual errors for elastico-viscous fluid considering optimal values of auxiliary parameters.

m	ε_m^f	ε_m^θ	ε_m^ϕ
2	3.75×10^{-5}	6.24×10^{-4}	9.80×10^{-5}
6	3.76×10^{-6}	4.15×10^{-5}	8.51×10^{-5}
10	1.33×10^{-6}	8.41×10^{-6}	7.95×10^{-5}
16	5.01×10^{-7}	1.49×10^{-6}	7.40×10^{-5}
20	3.22×10^{-7}	6.10×10^{-7}	7.14×10^{-5}

https://doi.org/10.1371/journal.pone.0174938.t001

Table 2. Individual averaged squared residual errors for second grade fluid considering optimal values of auxiliary parameters.

m	ε_m^f	ε_m^θ	ε_m^ϕ
2	8.83×10^{-7}	5.23×10^{-4}	1.32×10^{-4}
6	1.27×10^{-8}	2.46×10^{-5}	1.21×10^{-4}
10	6.63×10^{-9}	5.98×10^{-6}	1.14×10^{-4}
16	4.39×10^{-9}	3.15×10^{-6}	1.06×10^{-4}
20	3.42×10^{-9}	2.57×10^{-6}	1.02×10^{-4}

https://doi.org/10.1371/journal.pone.0174938.t002

Impacts of porosity parameter λ and inertia coefficient F_r on the non-dimensional velocity field $f'(\zeta)$ are plotted in Figs 3 and 4 respectively. Fig 3 depicts the impact of porosity parameter λ on velocity field $f'(\zeta)$ for both elastico-viscous and second grade fluids. An increment in the values of porosity parameter λ present decreasing trend in the velocity field $f'(\zeta)$ for both fluids. Physically the existence of porous media is to increase the resistance to fluid flow which causes decay in fluid velocity and related momentum layer thickness. Fig 4 presents change in velocity

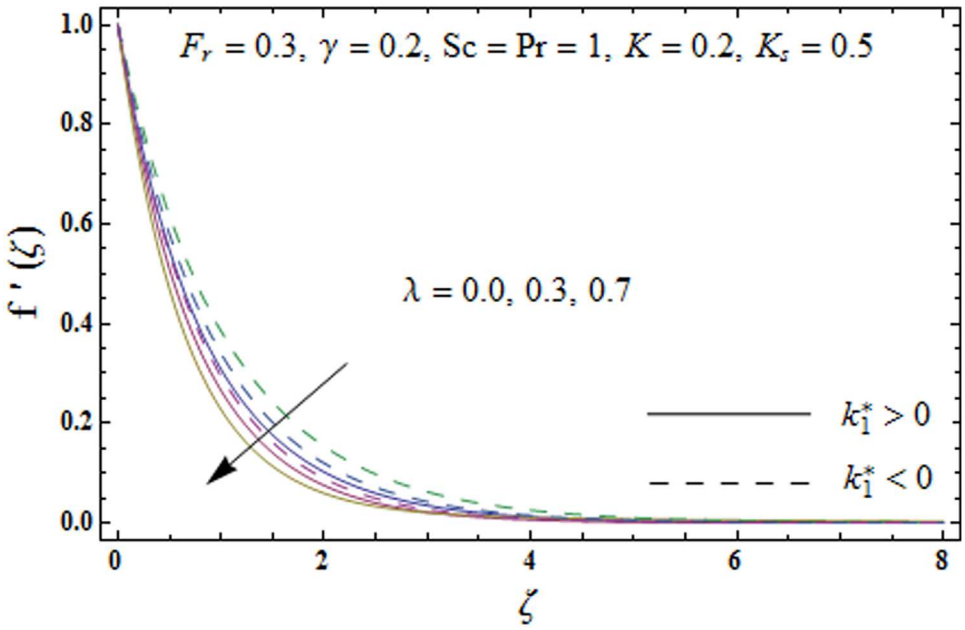

Fig 3. Plots of velocity field $f'(\zeta)$ for porosity parameter λ.

https://doi.org/10.1371/journal.pone.0174938.g003

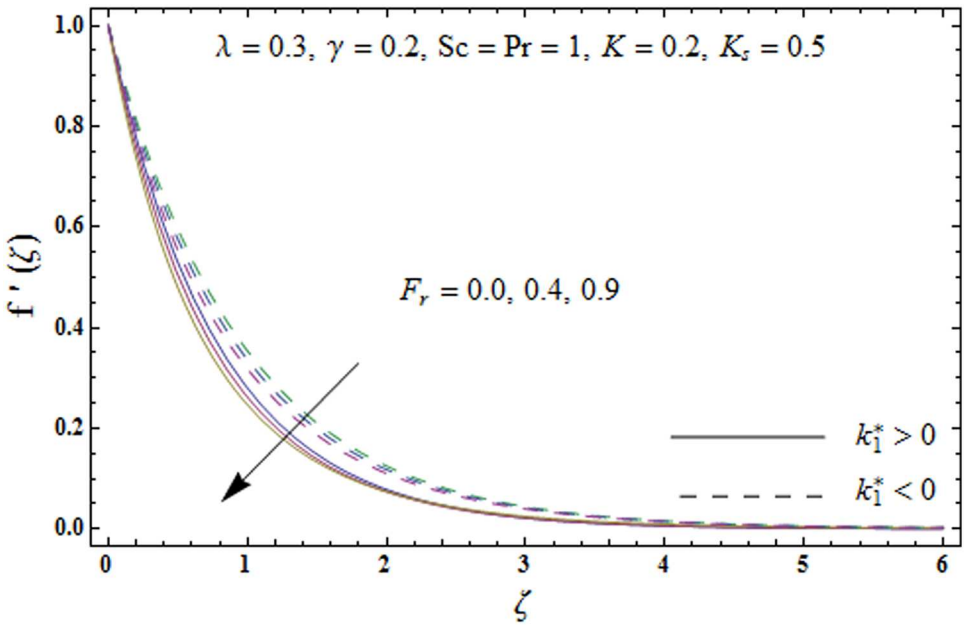

Fig 4. Plots of velocity field $f'(\zeta)$ for inertia coefficient F_r.

https://doi.org/10.1371/journal.pone.0174938.g004

field $f'(\zeta)$ for varying inertia coefficient F_r for both elastico-viscous and second grade fluids. It has been noticed that the velocity profile $f'(\zeta)$ reduces for higher values of inertia coefficient F_r.

Figs 5–8 are plotted to explore the impacts of porosity parameter λ, inertia coefficient F_r, thermal relaxation parameter γ and Prandtl number Pr on the non-dimensional temperature

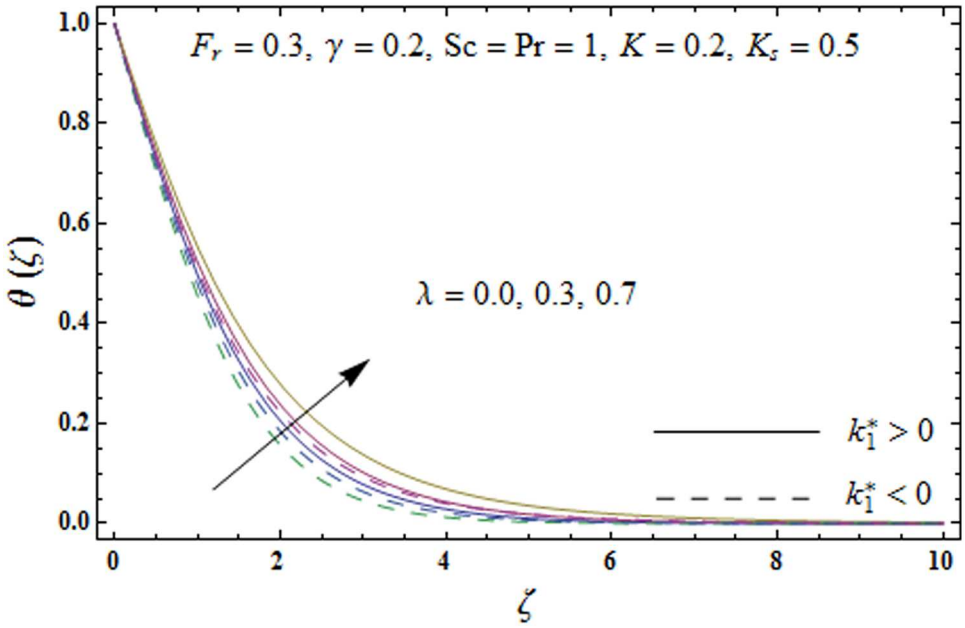

Fig 5. Plots of temperature field $\theta(\zeta)$ for porosity parameter λ.

https://doi.org/10.1371/journal.pone.0174938.g005

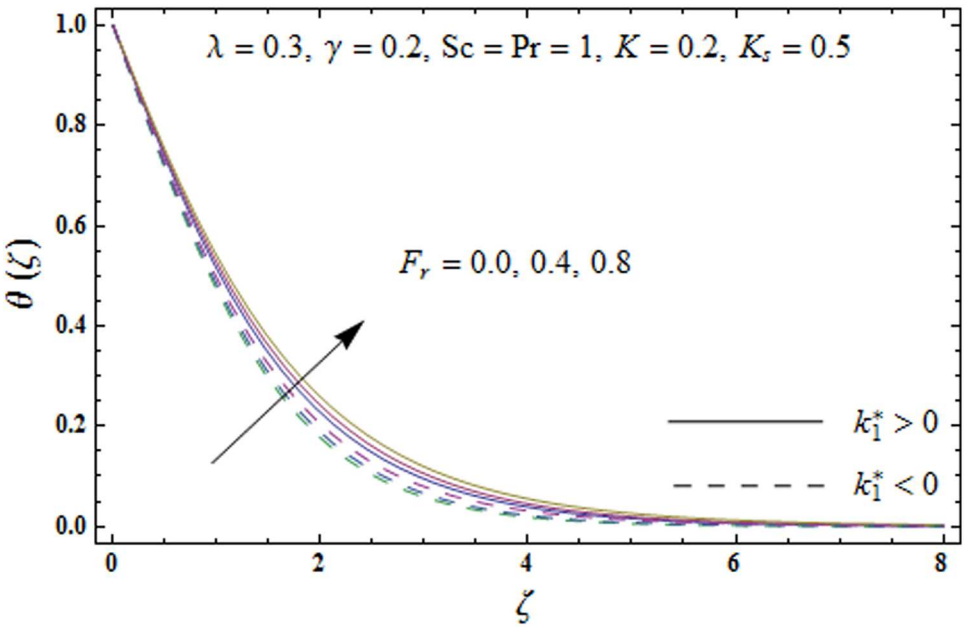

Fig 6. Plots of temperature field $\theta(\zeta)$ for inertia coefficient F_r.

https://doi.org/10.1371/journal.pone.0174938.g006

field $\theta(\zeta)$. Fig 5 displays the change in temperature field $\theta(\zeta)$. for varying porosity parameter λ. Higher values of porosity parameter λ correspond to stronger temperature field $\theta(\zeta)$ and more thermal layer thickness for both fluids. Fig 6 presents the effect of inertia coefficient F_r on temperature field $\theta(\zeta)$ It has been noticed that the temperature field $\theta(\zeta)$ and related thermal layer thickness are more for increasing values of inertia coefficient F_r for both fluids. Fig 7 presents that how Prandtl number Pr effect the temperature field $\theta(\zeta)$. It has been observed that the temperature field $\theta(\zeta)$ and thermal layer thickness are lower for increasing values of Prandtl number Pr for both elastico-viscous and second grade fluids Effect of thermal relaxation parameter γ on temperature field $\theta(\zeta)$ is sketched in Fig 8 for both fluids. Both temperature field $\theta(\zeta)$ and thermal layer thickness are reduced when thermal relaxation parameter γ increases.

Figs 9–13 are sketched to analyze the impacts of porosity parameter λ, inertia coefficient F_r, Schmidt number Sc, strength of homogeneous reaction K and strength of heterogeneous reaction K_s on the non-dimensional concentration field $\phi(\zeta)$. Fig 9 plots the concentration field $\phi(\zeta)$ for varying porosity parameter λ. It has been noticed that by increasing porosity parameter λ, a reduction in concentration field $\phi(\zeta)$ is observed for both elastico-viscous and second grade fluids Fig 10 depicts the effect of inertia coefficient F_r on concentration field $\phi(\zeta)$. Higher values of inertia coefficient F_r lead to weaker concentration field $\phi(\zeta)$ and less concentration layer thickness for both elastico-viscous and second grade fluids. Fig 11 demonstrates that how Schmidt number Sc effect the concentration field $\phi(\zeta)$. Concentration field $\phi(\zeta)$ shows increasing trend for larger Schmidt number Sc for both elastico-viscous and second grade fluids. Fig 12 shows that how strength of homogeneous reaction K effect the concentration field $\phi(\zeta)$ for both elastico-viscous and second grade fluids. It has been observed that larger K produces decreasing trend in concentration field $\phi(\zeta)$. Fig 13 depicts the impact of K_s on concentration field $\phi(\zeta)$ for both elastico-viscous and second grade fluids Larger K_s shows increasing trend for concentration field $\phi(\zeta)$.

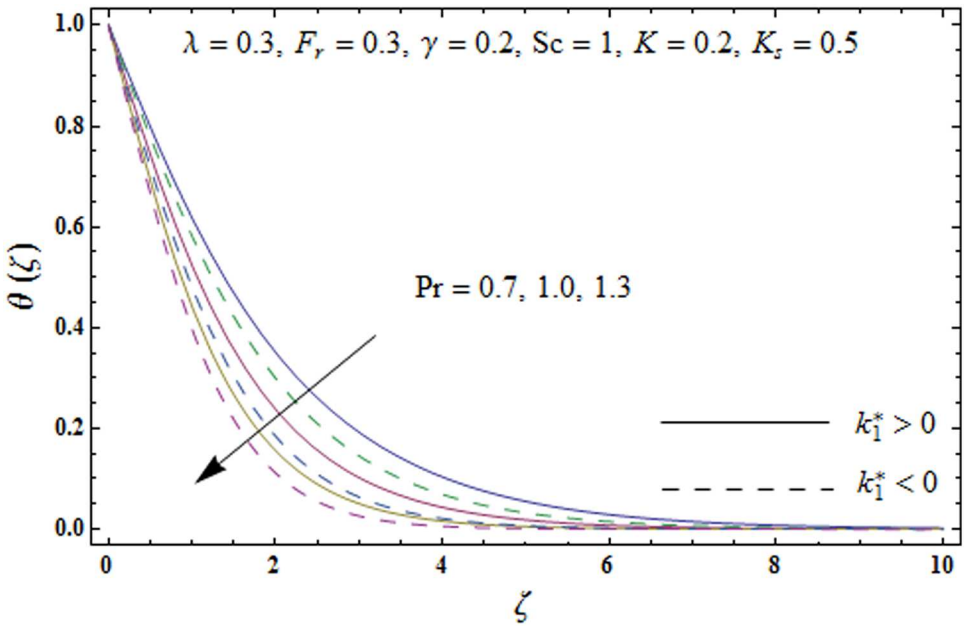

Fig 7. Plots of temperature field $\theta(\zeta)$ for Prandtl number Pr.

https://doi.org/10.1371/journal.pone.0174938.g007

Table 3 is arranged to analyze the skin friction coefficient $Re_x^{1/2}C_f$ for varying k_1^*, λ and F_r. It is noticed that the skin friction coefficient has higher values for larger porosity parameter λ and inertia coefficient F_r in the presence of both elastico-viscous and second grade fluids. Table 4 shows the comparison for different values of viscoelastic parameter k_1^* with homotopy

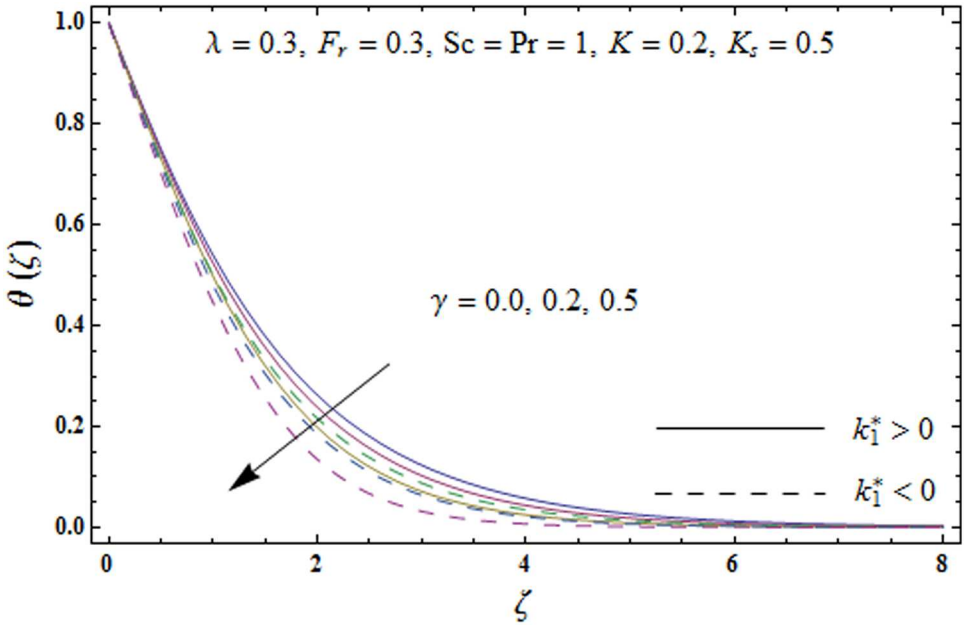

Fig 8. Plots of temperature field $\theta(\zeta)$ for thermal relaxation parameter γ.

https://doi.org/10.1371/journal.pone.0174938.g008

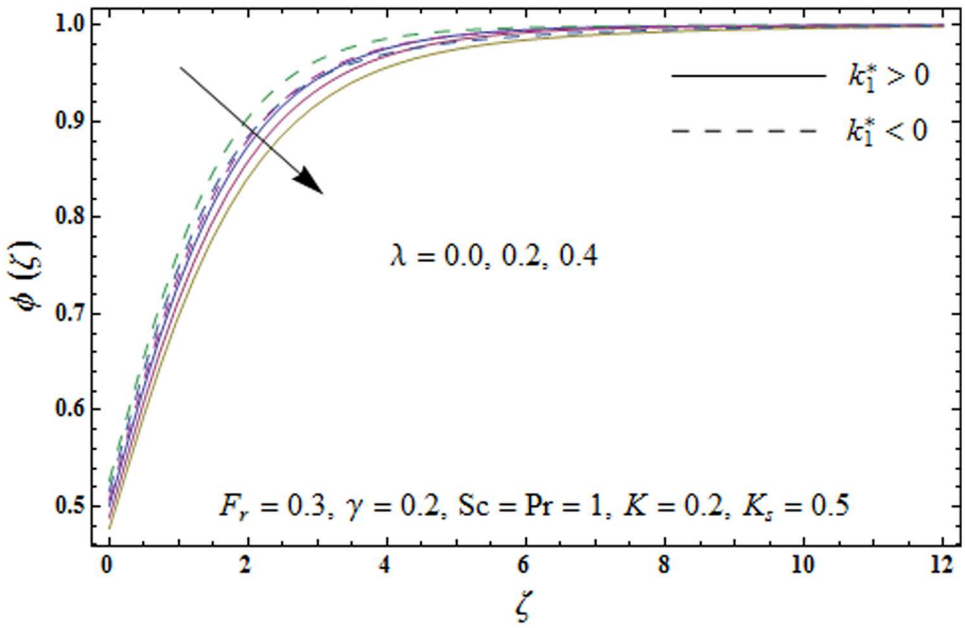

Fig 9. Plots of concentration field $\phi(\zeta)$ for porosity parameter λ.

https://doi.org/10.1371/journal.pone.0174938.g009

analysis method (HAM). Table 4 presents a good agreement of OHAM solution with the existing homotopy analysis method (HAM) solution in a limiting case. Tables 5 and 6 present the numerical data for local Nusselt number $-\theta'(0)$ for distinct values of γ for both elastico-viscous $\left(k_1^* > 0\right)$ and second grade $\left(k_1^* < 0\right)$ fluids respectively. Local Nusselt number is noted high via γ in the presence of both elastico-viscous and second grade fluids.

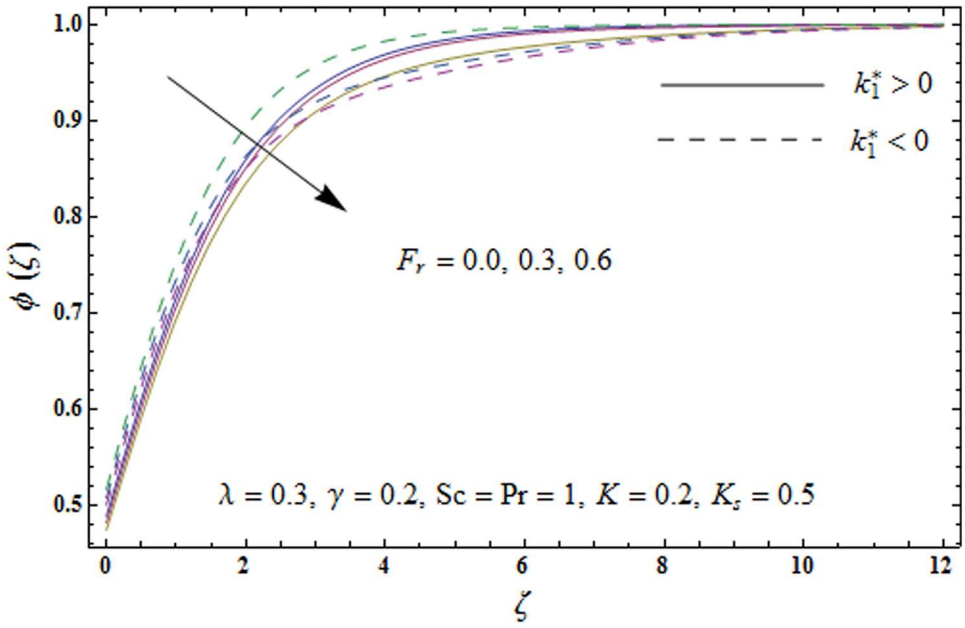

Fig 10. Plots of concentration field $\phi(\zeta)$ for inertia coefficient F_r.

https://doi.org/10.1371/journal.pone.0174938.g010

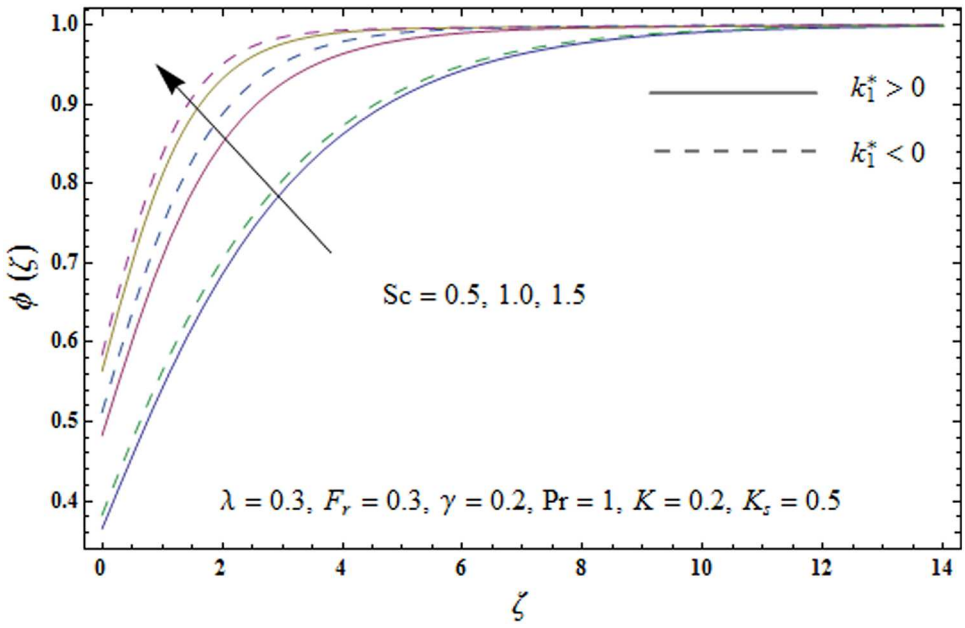

Fig 11. Plots of concentration field $\phi(\zeta)$ for Schmidt number *Sc*.

https://doi.org/10.1371/journal.pone.0174938.g011

6. Conclusions

Darcy-Forchheimer flow of viscoelastic fluids bounded by a linear stretchable surface with Cattaneo-Christov heat flux model and homogeneous-heterogeneous reactions has been discussed. The key findings of present investigation are listed below:

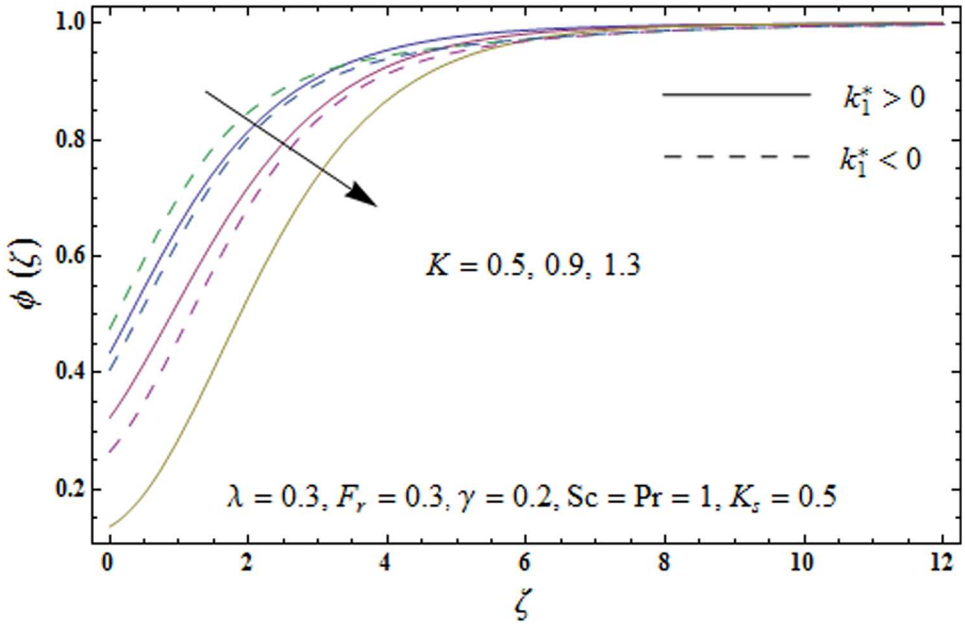

Fig 12. Plots of concentration field $\phi(\zeta)$ for strength of homogeneous reaction K_s.

https://doi.org/10.1371/journal.pone.0174938.g012

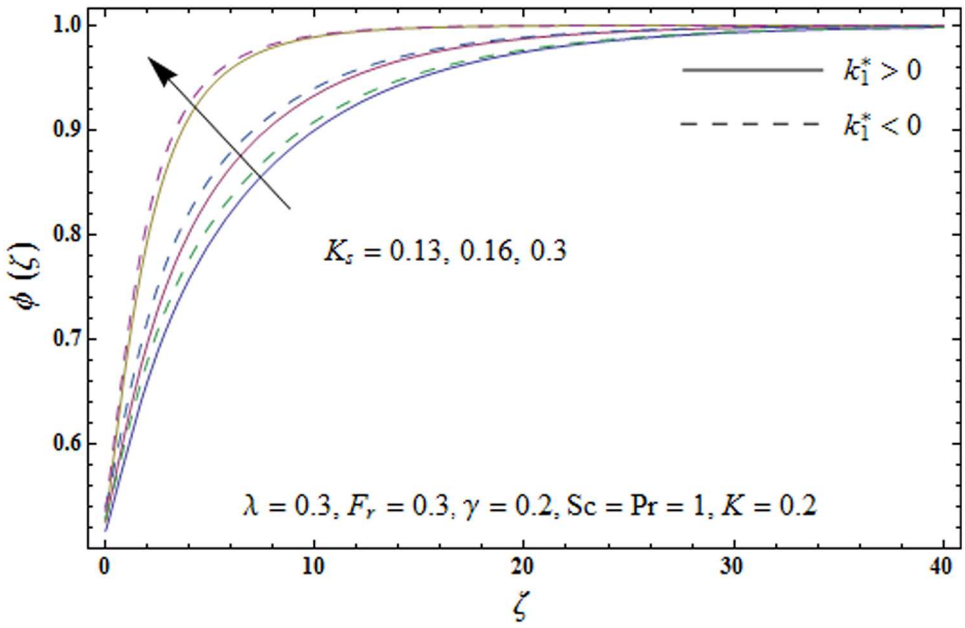

Fig 13. Plots of concentration field $\phi(\zeta)$ for strength of heterogeneous reaction K_s.

https://doi.org/10.1371/journal.pone.0174938.g013

Table 3. Numerical data for skin friction coefficient $-Re_x^{1/2}C_f$ for different values of k_1^*, λ and F_r.

		$-Re_x^{1/2}C_f$	$-Re_x^{1/2}C_f$
λ	F_r	$k_1^* = -0.2$	$k_1^* = -0.2$
0.0	**0.3**	1.5837	0.4934
0.1		1.6503	0.5134
0.2		1.7142	0.5327
0.3	0.0	1.6653	0.5099
	0.1	1.7028	0.5240
	0.2	1.7396	0.5378

https://doi.org/10.1371/journal.pone.0174938.t003

Table 4. Comparative values of $-Re_x^{1/2}C_f$ for different values of viscoelastic parameter k_1^* when $\lambda = F_r = 0$.

k_1^*	$-Re_x^{1/2}C_f$	
	OHAM	*HAM*[27]
0.0	1.00000	1.00000
0.1	0.73786	0.73786
0.2	0.44721	0.44721
0.3	0.11952	0.11952

https://doi.org/10.1371/journal.pone.0174938.t004

Table 5. Numerical data of local Nusselt number $-\theta'(0)$ in elastico-viscous fluid for different values of γ when $k_1^* = 0.2$, $\lambda = F_r = 0.3$, Pr = Sc = 1.0, K = 0.2 and K_s = 0.5.

γ	0.0	0.2	0.4	0.6	0.8
$-\theta'(0)$	0.5167	0.5299	0.5437	0.5586	0.5747

https://doi.org/10.1371/journal.pone.0174938.t005

Table 6. Numerical data of local Nusselt number $-\theta'(0)$ in second grade fluid for different values of γ when $k_1^* = -0.2$, $\lambda = F_r = 0.3$, Pr = Sc = 1.0, K = 0.2 and K_s = 0.5.

γ	0.0	0.2	0.4	0.6	0.8
$-\theta'(0)$	0.5653	0.5822	0.6001	0.6193	0.6411

https://doi.org/10.1371/journal.pone.0174938.t006

- Increasing values of porosity parameter λ and inertia coefficient F_r show reduction in the velocity field $f'(\zeta)$.
- Both temperature $\theta(\zeta)$ and concentration $\phi(\zeta)$ fields depict opposite behavior for larger porosity parameter λ.
- Larger values of inertia coefficient F_r lead to higher temperature field $\theta(\zeta)$ while opposite trend is noticed for concentration field $\phi(\zeta)$.
- Larger Prandtl number Pr and thermal relaxation parameter γ show decay in temperature $\theta(\zeta)$.
- An increment in Schmidt number Sc and strength of heterogenous reaction K_s leads to higher concentration field $\phi(\zeta)$.
- Larger strength of homogeneous reaction K causes a decay in the concentration field $\phi(\zeta)$.
- Skin friction coefficient for both fluids is higher for larger porosity parameter λ and inertia coefficient F_r.
- Local Nusselt number is increasing function of thermal relaxation parameter γ in cases of both fluids.

The present analysis provides a motivation for future developments on the topic in regimes of shrinking sheet, variable sheet thickness, variable thermal conductivity and Cattaneo-Christov double diffusion [60].

Author Contributions

Conceptualization: TH FH TM AA.

Data curation: TH FH TM AA.

Formal analysis: TH FH TM AA.

Investigation: TH FH TM AA.

Methodology: TH FH TM AA.

Project administration: TH FH TM AA.

Resources: TH FH TM AA.

Software: TH FH TM AA.

Supervision: TH FH TM AA.

Validation: TH FH TM AA.

Visualization: TH FH TM AA.

Writing – original draft: TH FH TM AA.

Writing – review & editing: TH FH TM AA.

References

1. Nield DA, Bejan A. Convection in porous media. Springer, New York, NY, USA 1999.
2. Karniadakis G, Beskok A. Micro flows. Springer, New York, NY, USA 2002.
3. Karniadakis G, Beskok A, Aluru N. Micro flows and nano flows: Fundamentals and simulation. Springer, New York, NY, USA 2005.
4. Forchheimer P. Wasserbewegung durch boden. Zeitschrift Ver D Ing. 1901; 45: 1782–1788.
5. Muskat M. The flow of homogeneous fluids through porous media. Edwards, MI 1946.
6. Seddeek MA. Influence of viscous dissipation and thermophoresis on Darcy-Forchheimer mixed convection in a fluid saturated porous media. J Colloid Interface Sci. 2006; 293: 137–142. https://doi.org/10.1016/j.jcis.2005.06.039 PMID: 16112126
7. Pal D, Mondal H. Hydromagnetic convective diffusion of species in Darcy-Forchheimer porous medium with non-uniform heat source/sink and variable viscosity. Int Commun Heat Mass Transfer. 2012; 39: 913–917.
8. Sadiq MA, Hayat T. Darcy-Forchheimer flow of magneto Maxwell liquid bounded by convectively heated sheet. Results Phys. 2016; 6: 884–890.
9. Shehzad SA, Abbasi FM, Hayat T, Alsaedi A. Cattaneo-Christov heat flux model for Darcy-Forchheimer flow of an Oldroyd-B fluid with variable conductivity and non-linear convection. J Mol Liq. 2016; 224: 274–278.
10. Hayat T, Muhammad T, Al-Mezal S, Liao SJ. Darcy-Forchheimer flow with variable thermal conductivity and Cattaneo-Christov heat flux. Int J Numer. Methods Heat Fluid Flow. 2016; 26: 2355–2369.
11. Akbar NS, Raza M, Ellahi R. Influence of heat generation and heat flux on peristaltic flow with interacting nanoparticles. Eur Phys J Plus. 2014; 129: 185.
12. Akbar NS, Raza M, Ellahi R. Influence of induced magnetic field and heat flux with the suspension of carbon nanotubes for the peristaltic flow in a permeable channel. J Magn Magn Mater. 2015; 381: 405–415.
13. Majeed A, Zeeshan A, Ellahi R. Unsteady ferromagnetic liquid flow and heat transfer analysis over a stretching sheet with the effect of dipole and prescribed heat flux. J Mol Liq. 2016; 223: 528–533.
14. Sheikholeslami M. Numerical simulation of magnetic nanofluid natural convection in porous media. Phys Lett A. 2017; 381: 494–503.
15. Sheikholeslami M. Magnetic field influence on nanofluid thermal radiation in a cavity with tilted elliptic inner cylinder. J Mol Liq. 2017; 229: 137–147.
16. Sheikholeslami M, Ganji DD. Impact of electric field on nanofluid forced convection heat transfer with considering variable properties. J Mol Liq. 2017; 229: 566–573.
17. Sheikholeslami M, Rokni HB. Numerical modeling of nanofluid natural convection in a semi annulus in existence of Lorentz force. Comp Methods Appl Mech Eng. 2017; 317: 419–430.
18. Sheikholeslami M, Shehzad SA. Thermal radiation of ferrofluid in existence of Lorentz forces considering variable viscosity. Int J Heat Mass Transfer. 2017; 109: 82–92.
19. Fourier JBJ. Théorie Analytique De La Chaleur. Paris 1822.
20. Cattaneo C. Sulla conduzione del calore. Atti Semin Mat Fis Univ Modena Reggio Emilia. 1948; 3: 83–101.
21. Christov CI. On frame indifferent formulation of the Maxwell-Cattaneo model of finite-speed heat conduction. Mech Res Commun. 2009; 36: 481–486.
22. Straughan B. Thermal convection with the Cattaneo-Christov model. Int J Heat Mass Transfer. 2010; 53: 95–98.
23. Ciarletta M, Straughan B. Uniqueness and structural stability for the Cattaneo-Christov equations. Mech Res Commun. 2010; 37: 445–447.
24. Haddad SAM. Thermal instability in Brinkman porous media with Cattaneo-Christov heat flux. Int J Heat Mass Transfer. 2014; 68: 659–668.
25. Mustafa M. Cattaneo-Christov heat flux model for rotating flow and heat transfer of upper-convected Maxwell fluid. AIP Adv. 2015; 5: 047109.
26. Hayat T, Farooq M, Alsaedi A, Al-Solamy F. Impact of Cattaneo-Christov heat flux in the flow over a stretching sheet with variable thickness. AIP Adv. 2015; 5: 087159.
27. Hayat T, Muhammad T, Alsaedi A, Mustafa M. A comparative study for flow of viscoelastic fluids with Cattaneo-Christov heat flux. Plos One. 2016; 11: e0155185. https://doi.org/10.1371/journal.pone.0155185 PMID: 27176779

28. Waqas M, Hayat T, Farooq M, Shehzad SA, Alsaedi A. Cattaneo-Christov heat flux model for flow of variable thermal conductivity generalized Burgers fluid. J Mol Liq. 2016; 220: 642–648.
29. Li J, Zheng L, Liu L. MHD viscoelastic flow and heat transfer over a vertical stretching with Cattaneo-Christov heat flux. J Mol Liq. 2016; 221: 19–25.
30. Hayat T, Muhammad T, Alsaedi A, Ahmad B. Three-dimensional flow of nanofluid with Cattaneo-Christov double diffusion. Results Phys. 2016; 6: 897–903.
31. Merkin JH. A model for isothermal homogeneous-heterogeneous reactions in boundary-layer flow. Math Comp Modell. 1996; 24: 125–136.
32. Chaudhary MA, Merkin JH. A simple isothermal model for homogeneous-heterogeneous reactions in boundary-layer flow. II Different diffusivities for reactant and autocatalyst. Fluid Dyn Res. 1995; 16: 335–359.
33. Bachok N, Ishak A, Pop I. On the stagnation-point flow towards a stretching sheet with homogeneous-heterogeneous reactions effects. Commun Nonlinear Sci Numer Simul. 2011; 16: 4296–4302.
34. Kameswaran PK, Shaw S, Sibanda P, Murthy PVSN. Homogeneous-heterogeneous reactions in a nanofluid flow due to porous stretching sheet. Int J Heat Mass Transfer. 2013; 57: 465–472.
35. Hayat T, Hussain Z, Alsaedi A, Ahmad B. Heterogeneous-homogeneous reactions and melting heat transfer effects in flow with carbon nanotubes. J Mol Liq. 2016; 220: 200–207.
36. Imtiaz M, Hayat T, Alsaedi A, Hobiny A. Homogeneous-heterogeneous reactions in MHD flow due to an unsteady curved stretching surface. J Mol Liq. 2016; 221: 245–253.
37. Hayat T, Qayyum S, Imtiaz M, Alsaedi A. Impact of Cattaneo-Christov heat flux in Jeffery fluid flow with homogeneous-heterogeneous reactions. Plos One. 2016; 11: e0148662. https://doi.org/10.1371/journal.pone.0148662 PMID: 26859675
38. Hayat T, Hussain Z, Muhammad T, Alsaedi A. Effects of homogeneous and heterogeneous reactions in flow of nanofluids over a nonlinear stretching surface with variable surface thickness. J Mol Liq. 2016; 221: 1121–1127.
39. Sajid M, Iqbal SA, Naveed M, Abbas Z. Effect of homogeneous-heterogeneous reactions and magnetohydrodynamics on Fe_3O_4 nanofluid for the Blasius flow with thermal radiations. J Mol Liq. 2017; 233: 115–121.
40. Tanveer A, Hayat T, Alsaedi A, Ahmad B. Mixed convective peristaltic flow of Sisko fluid in curved channel with homogeneous-heterogeneous reaction effects. J Mol Liq. 2017; 233: 131–138.
41. Hayat T, Hussain Z, Alsaedi A, Mustafa M. Nanofluid flow through a porous space with convective conditions and heterogeneous- homogeneous reactions. J Taiwan Inst Chem Eng. 2017; 70: 119–126.
42. Ariel PD. On the flow of an elastico-viscous fluid near a rotating disk. J Comput Appl Math. 2003; 154: 1–25.
43. Tan WC, Masuoka T. Stokes first problem for second grade fluid in a porous half space. Int J Non-Linear Mech. 2005; 40: 515–522.
44. Fetecau C, Fetecau C. Starting solutions for the motion of a second grade fluid due to longitudinal and torsional oscillations of a circular cylinder. Int J Eng Sci. 2006; 44: 788–796.
45. Turkyilmazoglu M. Multiple solutions of heat and mass transfer of MHD slip flow for the viscoelastic fluid over a stretching sheet. Int J Thermal Sci. 2011; 50: 2264–2276.
46. Turkyilmazoglu M. The analytical solution of mixed convection heat transfer and fluid flow of a MHD viscoelastic fluid over a permeable stretching surface. Int J Mech Sci. 2013; 77: 263–268.
47. Hayat T, Muhammad T, Shehzad SA, Alsaedi A. Similarity solution to three dimensional boundary layer flow of second grade nanofluid past a stretching surface with thermal radiation and heat source/sink. AIP Adv. 2015; 5: 017107.
48. Hayat T, Aziz A, Muhammad T, Alsaedi A, Mustafa M. On magnetohydrodynamic flow of second grade nanofluid over a convectively heated nonlinear stretching surface. Adv Power Tech. 2016; 27: 1992–2004.
49. Liao SJ. An optimal homotopy-analysis approach for strongly nonlinear differential equations. Commun Nonlinear Sci Numer Simulat. 2010; 15: 2003–2016.
50. Dehghan M, Manafian J, Saadatmandi A. Solving nonlinear fractional partial differential equations using the homotopy analysis method. Numer Meth Partial Diff Eq. 2010; 26: 448–479.
51. Malvandi A, Hedayati F, Domairry G. Stagnation point flow of a nanofluid toward an exponentially stretching sheet with nonuniform heat generation/absorption. J Thermodynamics. 2013; 2013: 764827.
52. Sheikholeslami M, Hatami M, Ganji DD. Micropolar fluid flow and heat transfer in a permeable channel using analytic method. J Mol Liq. 2014; 194: 30–36.

53. Turkyilmazoglu M. An effective approach for evaluation of the optimal convergence control parameter in the homotopy analysis method. Filomat. 2016; 30: 1633–1650.
54. Zeeshan A, Majeed A, Ellahi R. Effect of magnetic dipole on viscous ferro-fluid past a stretching surface with thermal radiation. J Mol Liq. 2016; 215: 549–554.
55. Hayat T, Khan MI, Imtiaz M, Alsaedi A, Waqas M. Similarity transformation approach for ferromagnetic mixed convection flow in the presence of chemically reactive magnetic dipole. Phys Fluids. 2016; 28: 102003.
56. Hayat T, Abbas T, Ayub M, Muhammad T, Alsaedi A. On squeezed flow of Jeffrey nanofluid between two parallel disks. Appl Sci. 2016; 6: 346.
57. Hayat T, Ullah I, Muhammad T, Alsaedi A. A revised model for stretched flow of third grade fluid subject to magneto nanoparticles and convective condition. J Mol Liq. 2017; 230: 608–615.
58. Hayat T, Muhammad T, Shehzad SA, Alsaedi A. An analytical solution for magnetohydrodynamic Oldroyd-B nanofluid flow induced by a stretching sheet with heat generation/absorption. Int J Thermal Sci. 2017; 111: 274–288.
59. Turkyilmazoglu M. Determination of the correct range of physical parameters in the approximate analytical solutions of nonlinear equations using the Adomian decomposition method. Mediterr J Math. 2016; 13: 4019–4037.
60. Turkyilmazoglu M. Equivalences and correspondences between the deforming body induced flow and heat in two-three dimensions. Phys Fluids. 2016; 28: 043102.